ELSEVIER

Tectonophysics 241 (1995) 99–119

TECTONOPHYSICS

Contact metamorphism and depth of emplacement of the Manaslu granite (central Nepal). Implications for Himalayan orogenesis

Stéphane Guillot [a,*], Patrick Le Fort [a], Arnaud Pêcher [a], Matthieu Roy Barman [b], Jean Aprahamian [a]

[a] *Institut Dolomieu, Université Joseph Fourier, 3800 Grenoble, France*
[b] *Institut de Physique du Globe de Paris, 75000 Paris, France*

Received 16 March 1993; revised version accepted 14 July 1994

Abstract

The Manaslu massif (central Nepal) provides a well-exposed example of a deeply eroded pluton: its contact aureole can be followed from the base to the top along medium- to low-grade (mesozonal to anchizonal) Tethyan metasediments. Contact metamorphic mineral assemblages and thermobarometric estimations suggest that the granite was emplaced at 18–21 km for the base and 9–13 km for the roof. Calculated temperatures within the aureole, at 550 ± 40°C, are compatible with the intrusion temperature of a leucogranitic magma. Microstructural evidence shows that the temperature remained high (> 500°C) at the base of the massif during and after granite emplacement, whereas towards the top of the granite deformation proceeded rapidly at lower temperature. Heating of the abundant calcareous rocks in the contact aureole released a local CO_2-rich fluid, whereas a H_2O- and boron-rich fluid seems to have pervaded the whole zone; this fluid is probably exsolved from the granitic melt during its crystallization. The depth of emplacement of the massif has an important implication for the reconstruction of the Himalayan geodynamic evolution, implying a burial of the Tethyan metasediments by a major refolding of the sedimentary cover or, more probably, by extensive development of the North Himalayan nappes towards the south for more than 70 km, before granite emplacement, i.e., before the Miocene. The young age of the granite and its depth of emplacement suggest a rapid tectonic denudation, in the order of 1 mm a^{-1}, probably by normal faulting north of the massif during its cooling.

1. Introduction

The plate tectonic framework of the Himalaya–Tibet region is well established (Patriat and Achache, 1984; Le Fort, 1989): initial collision between the India and Eurasian plates occurred in the Eocene (50 Ma) and was followed by convergence, thrusting and uplift continuing to the present day.

The northern part of the Indian plate has been imbricated by a series of major N-dipping, southward-verging thrusts with remarkable continuity along the Himalayan orogenic segment for some

* Corresponding author.
* Present address: Laboratoire de Pétrologie, Université Claude Bernard, 69622 Villeurbanne, France.

SSDI 0040-1951(94)00144-8

2000 km. Though the behaviour of the two major thrust systems, the Main Boundary Thrust (MBT) and the Main Central Thrust (MCT), is reasonably understood, knowledge of the North Himalayan thrust system is more poorly constrained, particularly the importance of nappe extension before its erosion during rapid exhumation of the Himalaya and the southern Tibetan plateau, since Miocene times (Harrison et al., 1992). Estimation of the depth of emplacement of the Higher Himalayan leucogranites (HHL) would be a good way to constrain the nappe extension. The HHL intrude the Higher Himalayan Sedimentary Series (HHSS) and develop contact aureoles that record the temperature and pressure of granite emplacement.

The HHL have been thoroughly investigated for their petrological and source characteristics [see Le Fort et al. (1987) for a more complete review]. Observations concerning their emplacement are far less abundant. Le Fort (1981) reports contact metamorphism with biotite, muscovite, staurolite and garnet in pelitic schists at the roof of the Manaslu pluton and wollastonite in calc-silicate gneisses towards the base (Colchen et al., 1986), whereas Stern et al. (1989) describe the development of andalusite in the metapelites at the top of the Gangotri leucogranite (Garhwal). Burg et al. (1984) have observed andalusite, staurolite and chloritoid in the metapelite and scapolite in metacalcareous rocks in the contact aureole of the granitic pods of southern central Tibet as Guillot et al. (1994a) in the aureole of the Kula–Kangri (eastern Tibet).

We focus on the Manaslu region of the Central Nepal Himalaya (Fig. 1). Preliminary data

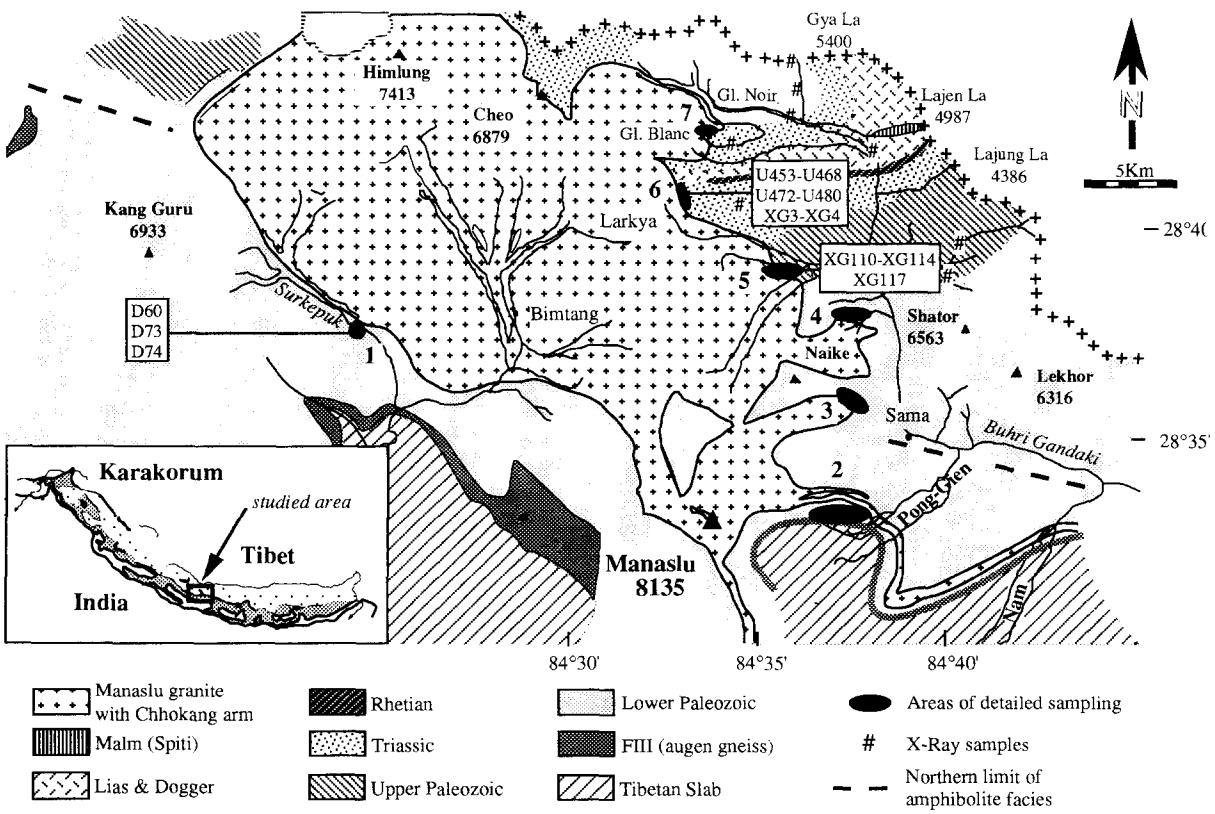

Fig. 1. Geological sketch map of the Manaslu massif, central Nepal (after Colchen et al., 1986). Samples discussed in text are reported on the map. The northern limit of the amphibolite grade regional metamorphism corresponds to the disappearance of sillimanite in pelitic rocks and clinopyroxene in the calcareous ones.

suggest that the Manaslu pluton was emplaced at depths of 8–15 km (France-Lanord and Le Fort, 1988; Copeland et al., 1990). The purpose of this paper is to present thermodynamic and microstructural analysis along the contact aureole of the Manaslu leucogranite (central Nepal), in order to evaluate the *P–T* conditions at the time of granite emplacement in the Higher Himalayan Sedimentary Series (HHSS).

2. Geological setting

The Manaslu leucogranite belongs to the belt of High Himalayan leucogranites recognized for some 1900 km from northern Pakistan to Bhutan. A dozen plutons and innumerable sheets and pods of smaller size lie on top of the Higher Himalayan Crystallines (HHC) and commonly intrude the Higher Himalayan Sedimentary Series (HHSS), the detached cover of the HHC.

According to the model of Le Fort (1981) supported by various studies (Vidal et al., 1982; Deniel et al., 1987; France-Lanord and Le Fort, 1988; England et al., 1992), the HHL originated by the melting of HHC pelitic gneisses by infiltration of fluid, at the time of thrusting along the Main Central Thrust (MCT).

The Manaslu pluton is Miocene on isotopic grounds using Rb/Sr whole-rock isochron and U/Pb dating on monazite (Deniel et al., 1987) favoured a crystallization age spanning the period from 25 to 18 Ma, whereas Copeland et al. (1990) with the addition of $^{39}Ar/^{40}Ar$ on micas proposed a restricted age of around 20 Ma and Guillot et al. (1994b) around 25 Ma. The granite is made up of xenomorphic quartz (32%), An_{21} to An_2 plagioclase (37%), K-feldspar (21%), muscovite (7%) and biotite (3%) and commonly contains abundant crystals of tourmaline (up to a few percent). The grain size is usually small (< 1 cm). The leucogranite is devoid of igneous enclaves and contains scarce xenoliths (Le Fort, 1991).

Outside the contact aureole, at the base of the HHSS, the metamorphic grade is high (amphibolitic grade) with diopside + K-feldspar parageneses in the metalimestones (Colchen et al., 1986) suggesting temperatures of up to 500°C (Schneider and Masch, 1993). The metamorphic grade decreases upwards from the upper Paleozoic to Dogger formations as demonstrated by fourteen samples collected in pelitic schist levels and analysed by X-ray diffractometry. The illite crystallinity decreases with the stratigraphic level, except for the two highest stratigraphic samples (Fig. 2A). However, the absence of paragonite in these samples attests of their low grade. The temperature can be roughly estimated between 300 and 350°C, with a primary paragenesis consisting of illite-chlorite-quartz ± paragonite ± mixed-layer of illite-paragonite ± plagioclase ± K-feldspar, corresponding to the lower-grade epizone (Frey, 1987). A retrograde assemblage appears in some samples, with chlorite-smectite or chlorite-vermiculite mixed-layer silicates and py-

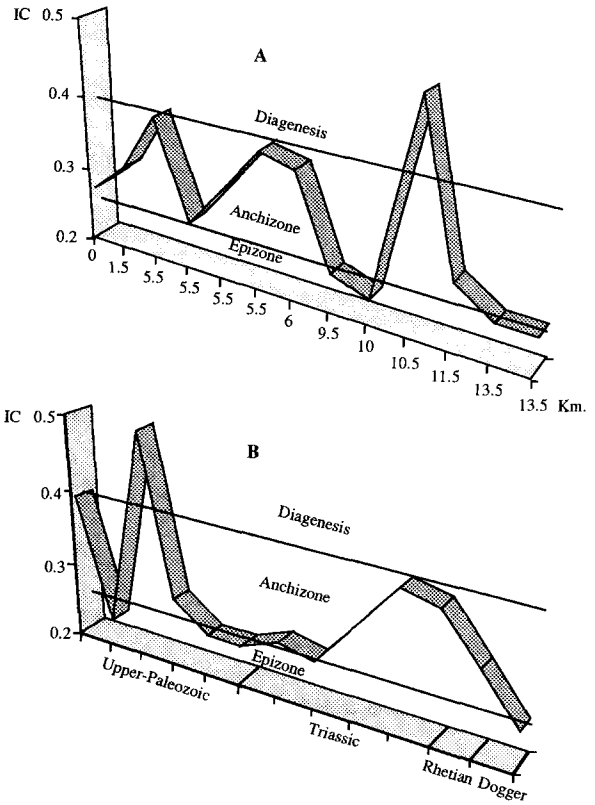

Fig. 2. Relationship between the illite crystallinity (Kübbler index, *IK*), the distance from the granite (A) and the stratigraphic level (B). The third sample of the upper Paleozoic is clearly retrogressed.

Table 1
Microprobe analyses of minerals used in thermobarometry

Contact:	1	1	1	1	1	1	1	1	1	1	1	1	1	6	6	6	6	6	6
Sample:	D73	D73	D73	D73	D60	D60	D60	D60	D60	D60	D74	D74	D74	D74	U453	U453	U453	U453	U468	U468
Mineral:	Grt	Bt	Pl	Ms	Grt	Bt	Pl	Ms	St	Grt	Bt	Pl	Ms	Grt	Bt	Pl	Ms	Grt	Bt
SiO_2	37.1	34.68	65.97	47.96	37.49	33.76	57.25	48.20	27.54	36.37	33.57	43.99	46.53	38.41	35.86	58.04	48.83	36.71	34.85
TiO_2	0.03	3.18	0	0.5	0	1.56	0	0.27	0.51	0.09	3.0	0.01	0.33	0.07	2.21	0	0.29	0	1.62
Al_2O_3	20.39	17.84	20.77	34.97	20.40	18.66	26.30	35.59	54.27	20.78	15.49	35.56	33.79	21.14	19.92	26.36	37.37	20.75	19.04
FeO	34.6	23.78	0.22	1.32	37.95	21.18	0.03	0.95	13.68	32.69	27.11	0	3.42	28.62	18.03	0.33	1.15	36.32	22.46
MnO	5.1	0.27	0	0.06	0.36	0	0	0.03	0.06	0.65	0.03	0	0.01	6.84	0.13	0.06	0.01	1.63	0
MgO	1.42	5.08	0	0.44	2.00	7.97	0.02	0.48	1.19	1.83	5.64	0	0.77	2.54	9.62	0	0.26	2.02	7.30
CaO	0.86	0	2.46	1.00	2.38	0	8.40	0	0.03	7.51	0	19.8	10.04	2.42	0.03	8.16	0	2.25	0
Na_2O	0	0.09	10.23	0.66	0	0.29	6.97	0.96	0.06	0	0.01	0.37	0.27	0	0.20	6.71	1.25	0	0.02
K_2O	0	9.18	0.10	10.06	0	8.80	0.06	9.67	0	0	9.06	0.02	10.34	0.01	8.52	0.05	8.56	0	8.58
Total	99.5	94.42	99.79	96.02	100.62	92.21	99.05	96.16	97.34	99.91	94.0	99.80	95.51	100.05	94.52	99.71	97.72	99.68	93.88
Oxy	24	22	8	22	24	22	8	22	31	24	22	8	22	24	22	8	22	24	22
Si	6.09	5.59	2.91	6.31	6.05	5.47	2.59	6.31	7.29	5.84	5.7	2.16	6.22	6.18	5.51	2.61	6.13	5.97	5.52
Ti	0	0.39	0	0.05	0	0.19	0	0.03	0.1	0.01	0.8	0	0.03	0.01	0.26	0	0.22	0	0.20
Al(IV)	0	2.41	0	3.73	0	2.53	1.41	1.69	16.94	0.16	2.51	1.84	1.78	0	2.49	1.39	1.87	0.03	2.53
Al(VI)	4.03	0.98	0	0	3.93	1.04	0	3.78	0	3.78	0.57	0	3.54	4.19	1.12	0	2.02	3.95	1.10
Fe	4.76	3.23	1.08	0.12	5.12	2.87	0	0.38	3.03	4.39	3.82	0	0.12	3.85	2.32	0.01	0.16	4.94	3.04
Mn	0.71	0	0	0.01	0.05	0	0	0.12	0.47	0.09	0	0	0	0.93	0	0	0	0.22	0
Mg	0.35	1.22	0	0.01	0.48	1.93	0	0	0.01	0.44	1.42	0	0.15	0.61	2.20	0	0.03	0.49	1.76
Ca	0.15	0	0.11	0.09	0.41	0	0.41	0.09	0.03	1.29	0	0.87	0	0.42	0.02	0.39	2.37	0.39	0
Na	0	0.03	0.87	0.17	0	0.09	0.61	0.24	0	0	0	0.14	0.07	0	0.06	0.58	0.04	0	0
K	0	1.89	0	1.69	0	1.82	0	1.61	0	0	1.95	0	1.76	0	1.67	0	1.83	0	1.77
	Alm 79.6 X_{Fe} 0.72 Ab 88 An 12				Alm 84.5 X_{Fe} 0.6 Ab 60 An 40					Alm 70.7 X_{Fe} 0.54 Ab 14 An 86				Alm 66.3 X_{Fe} 0.60 Ab 60 An 40				Alm 81.7 X_{Fe} 0.60	
	Grs 2.5 Prp 5.8				Grs 6.8 Prp 7.2					Grs 20.8 Prp 7.0				Grs 7.2 Prp 10.5				Grs 6.5 Prp 8.1	

Contact:	6	6	6	6	6	6	6	6	6	6	6	6	6	6	6	6	6	6	6
Sample:	U468	U468	U468	U472	U472	U472	U472	U480	U480	U480	U480	U480	XG3	XG3	XG3	XG4	XG4	XG4	XG4
Mineral:	Pl	Ms	St	Grt	Bt	Pl	Ms	Grt	Bt	Pl	Ms	St	Grt	Bt	Pl	Grt	Bt	Pl	Ms
SiO_2	60.49	48.91	28.29	37.12	35.67	59.57	49.03	36.61	35.68	60.67	46.46	28.4	37.73	35.92	59.61	36.48	35.58	67.04	46.88
TiO_2	0	0.26	0.47	0	1.22	0	0.25	0.9	1.5	0	0.39	0.3	0.06	2.18	0	0.09	1.13	0.02	0.02
Al_2O_3	24.84	36.90	55.3	20.62	19.41	25.16	36.49	20.24	19.83	24.30	36.60	54.62	21.17	19.02	25.63	21.58	19.05	20.44	30.97
FeO	0.17	1.24	11.32	33.81	21.65	0.17	1.23	33.63	19.96	0	1.33	11.71	30.83	18.39	0.16	30.65	20.41	0	6.77
MnO	0.01	0	0.11	2.82	0	0.12	0.01	6.16	0.13	0	0.08	0.04	6.18	0.18	3	6.37	0.27	0	0.11
MgO	0	0.41	1.03	2.09	8.42	0	0.57	1.88	8.46	0	0.66	1.00	2.60	9.43	0	2.49	8	0	2.15
CaO	6.67	0	0	3.07	0	6.99	0	1.23	0.03	6.14	0	0	1.88	0	7.85	2.14	0	1.96	0.03
Na_2O	7.61	1.04	0.04	0.08	0.06	7.54	0.55	0	0.07	8.44	0.76	0	0.0	0.16	7.16	0.01	0.08	10.18	0.26
K_2O	0.05	8.81	0	0	8.12	0.06	8.56	0	8.73	0.11	10.05	0	0.0	8.56	0.07	0.01	8.54	0.116	9.79
Total	99.26	97.57	96.56	99.60	94.57	99.61	96.69	100.65	94.39	99.69	96.33	96.07	100.45	93.87	100.55	99.02	93.08	99.77	96.98
Oxy	8	22	31	24	22	8	22	24	22	8	22	31	24	22	8	24	22	8	22
Si	2.69	6.27	8.17	6.02	5.58	2.67	6.32	5.98	5.56	2.70	6.10	8.26	6.06	5.58	2.65	5.96	5.64	2.94	6.25
Ti	0	0.03	0.1	0	0.14	0	0.02	0.01	0.18	0	0.04	0.07	0.01	0.26	0	0.01	0.13	0	0
Al(IV)	1.31	1.73	18.82	0	2.42	1.32	1.68	0	2.44	1.28	1.90		0.0	2.42	1.34	0.04	2.36	1.05	1.75
Al(VI)	0	3.84	0	3.96	1.16	0	3.86	3.88	1.2	0	3.77	18.71	4.06	1.06	0	3.92	1.2	0	3
Fe	0	0.12	2.73	4.59	2.83	0	0.12	4.60	2.6	0	0.12	2.85	4.14	2.39	0	4.18	2.71	0	0.13
Mn	0	0	0.03	0.39	0	0	0	0.85	0	0	0.01	0.01	0.84	0.02	0	0.88	0.04	0	0.01
Mg	0	0.08	0.44	0.51	1.96	0	0.11	0.46	1.96	0	0.13	0.43	0.62	2.18	0	0.60	1.89	0	0.45
Ca	0.32	0	0	0.53	0	0.33	0	0.22	0.02	0.30	0	0	0.32	0	0.37	0.37	0	0.09	0
Na	0.66	0.26	0.02	0	0.02	0.65	0.14	0	0.02	0.74	0.19	0	0.0	0.05	0.61	0	0.03	0.86	0.07
K	0	1.44	0	0	1.62	0	1.41	0	1.73	0.01	1.68	0	0.0	1.7	0	0	1.73	0	1.74
	An 67			Alm 76.2	X_{Fe} 0.57	Ab 66		Alm 75.1	X_{Fe} 0.54	Ab 71			Alm 69.9	X_{Fe} 0.5	Ab 62	Alm 69.2	X_{Fe} 0.56	Ab 90	
	An 33					An 34				An 29					An 38			An 10	
				Grs 8.9				Grs 3.5					Grs 5.4			Grs 69.2			
				Prp 8.4				Prp 7.5					Prp 9.5			Prp 10.0			

Electron microprobe analyses were performed on a Cameca CAMEBAX microprobe at the Polytechnic National Institute of Grenoble. The accelerating potential was 15kV. for a sample current of 10 nA and the counting time 5 s. Standards were natural silicates and oxides. Mineral abbreviations are from Kretz (1983).

rophyllite ± kaolinite. There is apparently no relationship between illite crystallinity and the mappable distance from the sample to the granite (Fig. 2B).

Close to the granite (< 100 m), the metasediments are strongly metamorphosed defining a contact aureole. The contact of the granite with the metasedimentary series has been followed discontinuously from lower Paleozoic to Dogger for a S–N distance of about 25 km. Seven principal contact zones have been studied and sampled (Fig. 1), two at the floor of the granite in the Surkepuk (contact 1) and Pong-Gien (contact 2) valleys, three others on the flank of the granite, along the eastern side of the Buhri Gandaki valley (contacts 3–5), and finally two at the roof of the pluton (contacts 6 and 7).

3. Chemistry / deformation relationships

Garnet and staurolite in the Triassic pelitic mica-schists were interpreted as synkinematic minerals by Le Fort (1981). Guillot et al. (1991) show, however, a more complex relationship between crystallization and deformation in the Manaslu aureole. In this section, we present a microstructural analysis and mineral chemistry of the contact metamorphic minerals of the calc-silicate gneisses, calcareous metasandstones and pelitic schists at the different contacts. Analyses of garnet, biotite, muscovite and plagioclase rim composition for the metapelitic schists are reported in Table 1. Mineral abbreviations are from Kretz (1983).

3.1. Contacts 1 and 2 at the floor of the pluton

The lower part of the Manaslu pluton intrudes two previously metamorphosed formations of the lower Paleozoic: the black Sanctuary and yellow Annapurna formations (Colchen et al., 1986). Both formations are made up of alternations, several centimeters to decimeters in thickness, of more pelitic and greywacke levels for the Sanctuary Formation where contact 1 is located, and

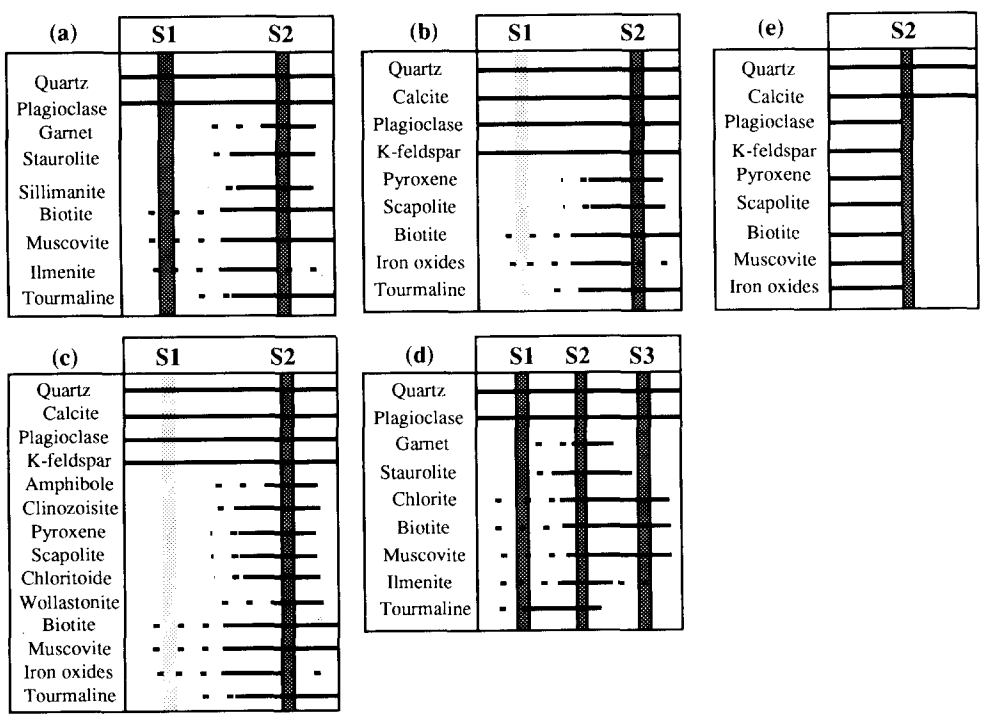

Fig. 3. Mineral crystallizations vs. deformations deduced from microscopic analyses of thin sections described in the text. (a) contact 1. (b) Contact 2. (c) Contact 3–5. (d) Contact 6. (e) Contact 7.

dominantly calc-silicate and marble rich for the Annapurna Formation, where we observed contact 2. Because of the apparent metamorphic continuity from the granite to the surrounding rocks, we are not able to distinguish the contact metamorphism from the regional metamorphism in this lower portion of the pluton. However, at contact 1, where the contact itself is only partly exposed, the pelitic schists contain two successive parageneses (Fig. 3a). The previous one consists of inclusion trails of biotite and muscovite in plagioclase, and crystallographically oriented arrays of acicular quartz inclusions in garnet and staurolite, probably related to a precursor foliation (S_1). The second assemblage defines the main foliation (S_2) with elongated porphyroblasts of garnet and staurolite surrounded by oriented flakes of biotite, muscovite and fibrous sillimanite. Fibrous sillimanite in the foliation plane S_2 locally grew at the expense of relic S_1 minerals (kyanite?), and defines a mineral SW–NE-striking lineation, perpendicular to the contact. Foliation S_2 dips at variable angle towards the North, parallel to the contact with the granite. Geometric relationships lead us to ascribe the second paragenesis to contact metamorphism and foliation S_2 to pluton emplacement.

Biotite composition relates to its microstructural position: the S_1 brown porphyroblasts have a X_{Fe} ratio of around 0.6 and a Ti content ranging from 0.18 to 0.25 atoms per 22 oxygens, whereas the S_2 biotites show the highest Ti content around 0.3–0.4 atoms and a X_{Fe} ratio around 0.7 (sample D74, Table 1). All white micas are essentially muscovite, with very small amounts of paragonite (Na content less than 0.4 atoms per formula unit, correlates with K content). Compositional variations are mainly reflected in the Si–Al correlation, close to the muscovite–phengite join. The most phengitic white mica is associated with the S_2 Fe-rich biotite, suggesting a lower temperature of crystallization or higher pressure (Massone and Schreyer, 1987).

Garnet usually shows a flat compositional profile (Fig. 4a), and not the distinctive bell-shape of contact metamorphic growth, such as reported by

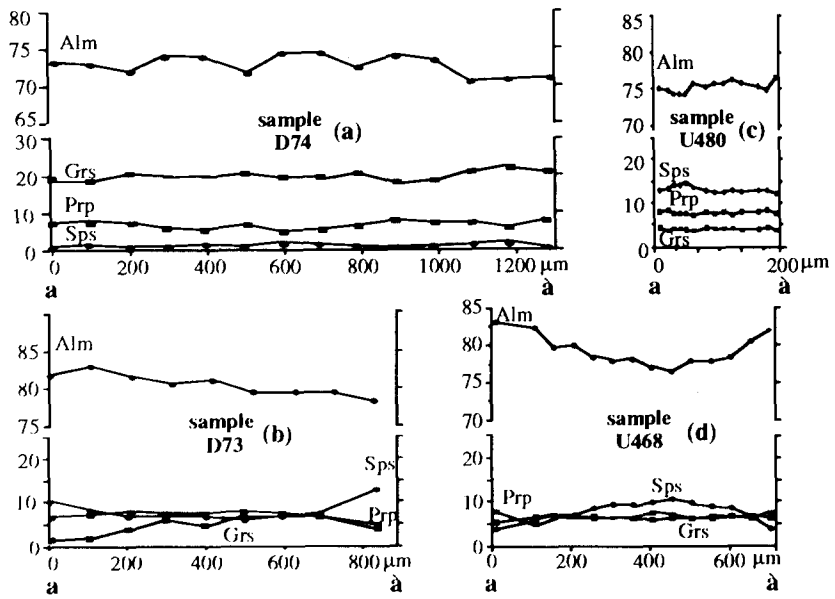

Fig. 4. Microprobe profiles across garnet crystals (see Fig. 5). (a) Pelitic schist with interlayered centimetric intercalations of calc-silicate gneisses, on rim contact with muscovite and biotite (sample D74, contact 1); the high grossular content relates to the calc-silicate layer vicinity. (b) Sillimanite-garnet pelitic schist, on rim contact with biotite ± sillimanite (sample D73, contact 1). (c) Chlorite-garnet-staurolite pelitic schist, in rim contact with biotite (sample U480, contact 6). (d) Staurolite-garnet pelitic schist, in rim contact with staurolite (sample U468, contact 6).

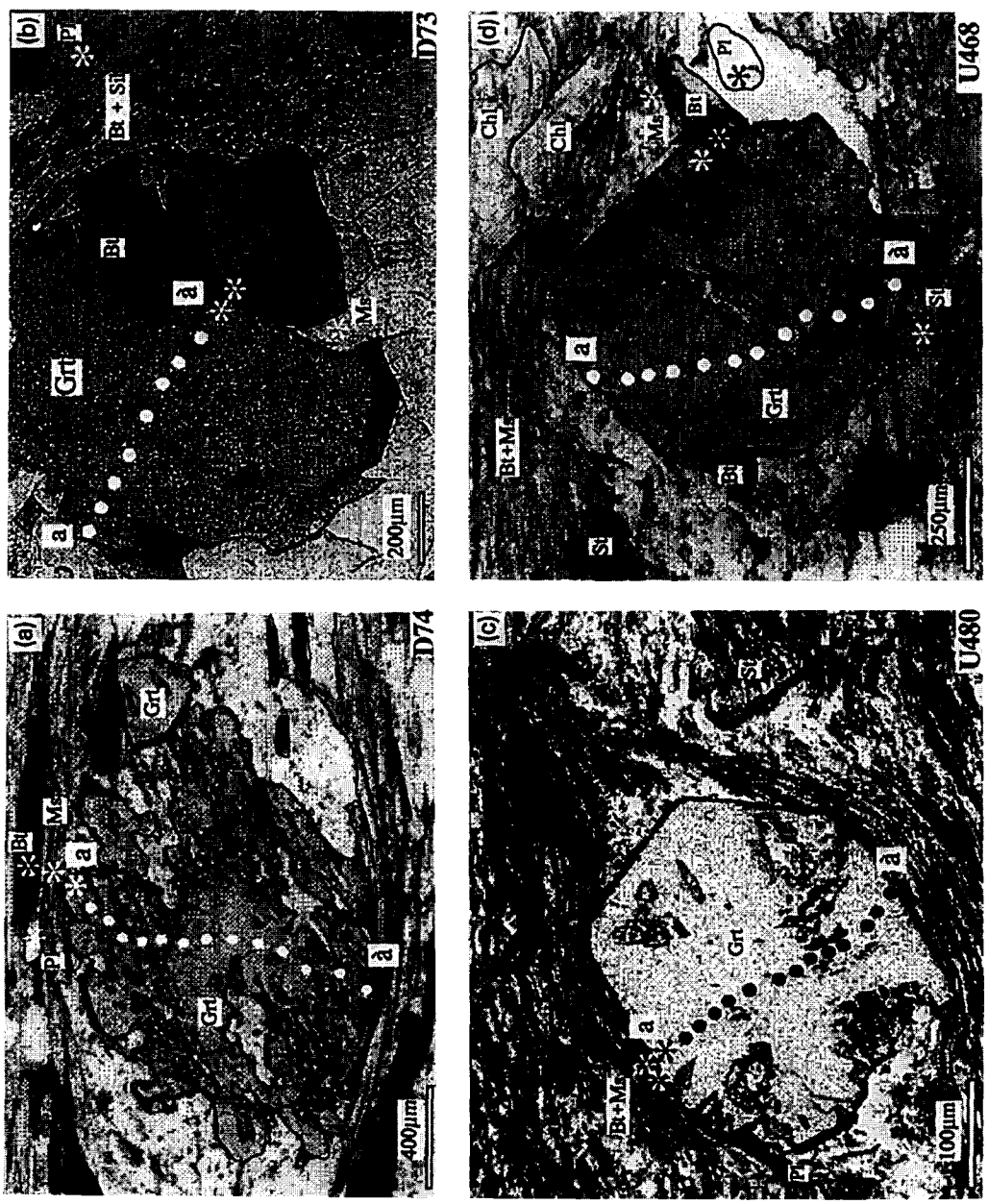

Fig. 5. Photomicrographs of the samples used for microprobe profiles showed on Fig. 5. Dots correspond to the microprobe profile analyses whereas stars correspond to analyses of Table 1. (a) Sample D74: the internal schistosity of the garnet corresponds to S_1, whereas the Bt + Ms foliation corresponds to S_2. (b) Sample D73: the Bt + Sil fabric is related to reaction (1a). (c) Sample U480. (d) Sample U468. Label a–$\grave{a}$ refers to Fig. 4.

Hollister (1969). Such flat profile probably reflects absence of P–T variations during garnet growth in absence of staurolite under rapid contact metamorphic conditions, rather than post-metamorphic cationic diffusion such as presented by Florence and Spear (1989). This is particularly conspicuous for sample D74 (Fig. 4a) in which the size of the garnet (> 1 cm) would preclude total homogeneization. However, in the sillimanite-bearing schists (Fig. 5b) at the same contact (D73), a slight reverse zonation marked by a decrease in almandine content and an increase in spessartine content (Fig. 4b) probably suggests the destabilisation of the rim of the garnet during the development of the following reactions:

$$\mathrm{Grt + Chl + Ms + Qtz = Bt + Sil + H_2O} \quad (1a)$$

$$\mathrm{Grt + Ms + Qtz = Bt + Sil} \quad (1b)$$

These reactions are actually observed in thin section by the development of biotite and sillimanite around garnet in the presence of muscovite and quartz.

The S_2 staurolite of sample D60, has a steady composition with a TiO_2 content of around 0.5 wt.% and a X_{Fe} ratio between 0.85 and 0.90.

The composition of the plagioclase relates essentially to the rock composition and its mineral assemblage: from very calcic (An_{80}–An_{90}) in the grossular-rich schist (D74), to intermediate (An_{25}–An_{45}) in the staurolite-rich rock (D60), and quite albitic (An_{10}–An_{15}) in the sillimanite-bearing schist (D73).

The calc-silicate gneisses are abundant at contact 2. They contain clinopyroxene, K-feldspar, plagioclase, quartz, biotite, muscovite, ± phlogopite, wollastonite, scapolite, tourmaline and accessory minerals (iron oxides, sphene, zircon). The foliation plane S_2 is parallel to the compositional layering (Fig. 3b) of clinopyroxene-K-feldspar-quartz and calcite-quartz ± scapolite, and the preferred orientation of elongate clinopyroxene defines a lineation. Calcite and quartz show a mosaic structure with few subgrains and a weak undulatory extinction, and commonly show triple junction indicating a secondary static recrystallization at high temperature.

Clinopyroxene consists of a homogeneous diopside-hedenbergite solid solution with a X_{Fe} [Fe/(Fe + Mg)] ratio ranging from 0.2 to 0.4 (salite). Scapolite has a uniform meionite ($Ca_4Al_6Si_6O_{24}$, CO_3) content [Ca/(Ca + Na + K)] of 75–80%. According to Moecher and Essene (1991), such mizzonitic composition is typical of the upper amphibolite to granulite facies. In terms of equivalent anorthite content, the scapolite corresponds to 58–63% EqAn [$= 100 \cdot (Al - 3)$], according to Shaw (1960) and Ellis (1978). K-feldspar is widespread, and plagioclase is oligoclase-andesine (An_{25}–An_{40}). Calc-silicate rocks locally contain biotite with the same composition as that of the pelitic schists. However, phlogopite is more common, with a X_{Fe} ratio ranging from 0.12 to 0.16.

3.2. Contacts 3, 4, 5 on the flank of the pluton

Lateral contacts occur in the Paleozoic series and, for all three of them, show predominantly calc-silicate gneisses and calcareous metasandstones with few levels of metagreywackes. Outside of the contact aureole, on a first approximation, let us recall that there is a strong decrease in the regional metamorphic grade from amphibolite facies at the level of contact 3, to greenschist at that of contact 4, and low grade at that of contact 5.

The calcareous metasandstones consist of abundant quartz, clinozoisite, amphibole, plagioclase ± biotite, muscovite, tourmaline, scapolite, K-feldspar, sphene and calcite. The compositional layering of quartz-amphibole and quartz-clinozoisite defines the weak foliation plane (S_2) oblique on the bedding structure (Fig. 3c). On S_2, a well-developed stretching lineation is marked by the elongation of pyrite or ilmenite oriented N70–80°E, dipping 15–30° eastward.

The amphibole in the calcareous metasandstones is homogeneous with a high Al content, around 1.5 atoms per formula unit, and relatively close to the tschermakite–pargasite join; using the classification of Leake (1978), it corresponds to ferroan pargasitic hornblende. Epidote is always associated with amphibole and corresponds to the clinozoisite endmember. The plagioclase is calcic (An_{60}–An_{97}). Rare scapolite occurs in

metasandstones, with a composition often similar to those of the calc-silicate gneisses, except for one sample (XG114, contact 5), in which scapolite is even more calcic, with 88% meionite content, suggesting a local CO_2-rich fluid. Titanite and hematite are common.

At contact 5, some metapelitic layers have a biotite-muscovite-quartz assemblage. The biotite is iron rich ($X_{Fe} = 0.65–0.75$) and the Ti concentration is high (> 0.35). Usually, in the pelitic schists high X_{Fe} ratios are associated with high Ti contents and correspond to high temperature (Kwak, 1968; Stephenson, 1977; Schreurs, 1985). But in this case, the unusual composition of the biotite, together with the absence of garnet or staurolite, may be related to the high initial Fe/Al ratio of these rocks.

The calc-silicate gneisses are very similar to those of the lower contacts, wollastonite only occurs in contact 4 in quartz- and calcite-rich layers.

3.3. Contact 6 at the roof of the pluton

This contact (between 20 and 100 m in thickness) is somewhat difficult to reach because of the altitude (between 5000 and 6000 m) and the steepness of the slopes (cf. fig. 4d in Le Fort, 1981). At the level we reached, the granite intrudes only Triassic alternances of sandstones, shales and shelly limestones. In the pelitic beds, we have distinguished three parageneses of increasing grade in the aureole:

—garnet + chlorite + biotite + muscovite + plagioclase + quartz (U472);
—garnet + biotite + muscovite + plagioclase + quartz (U453, XG3, XG4);
—garnet + staurolite + biotite + muscovite + plagioclase + quartz ± chlorite (U468, U480).

In the first assemblage, garnet and chlorite appear as porphyroblasts surrounded by a muscovite-biotite foliation. In the quartz-rich layer, an earlier schistosity defined by the aligment of previous biotite and muscovite is micro-folded and transposed into the new cleavage.

In the second assemblage, idioblastic garnet is surrounded by a muscovite-biotite foliation.

In the third assemblage, the staurolite commonly appears after the garnet. In places, the internal schistosity of the elongated staurolite passes into the main cleavage, suggesting the growth of staurolite during and after its development (Fig. 3d).

In all three assemblages, tourmaline and ilmenite are included within garnet and staurolite or associated with biotite and muscovite in the main cleavage. Tourmaline is elongated and broken in the foliation with crystallization of biotite and chlorite in the cracks.

A crenulation cleavage, oblique on the main one, is associated with the growth of a second generation of chlorite in the garnet-chlorite and garnet-biotite rocks. In the staurolite-bearing rocks, the crenulation cleavage is associated with the last increment of staurolite growth, and the recrystallisation of muscovite and biotite in the crenulation.

Garnet usually shows increasing almandine, and decreasing spessartine content from core to rim, while the grossular and pyrope contents remain almost constant. The MgO content varies from 5 to 10 wt.% and that of CaO from 3 to 7 wt.%. One staurolite-bearing sample (U480) shows homogeneous garnet (Fig. 4c) suggesting a rapid crystal growth at rather constant temperature or, considering the small size of the analysed crystals (around 225 μm), more probably cationic homogenization of the garnet during or after the peak of metamorphism (Spear, 1988; Florence and Spear, 1989). In biotite- and/or staurolite-bearing schists, the size of the garnet crystals is larger (up to 750 μm) and their almandine and spessartine zonation (Fig. 4d) could represent cationic exchange during biotite/staurolite growth or relict growth zonation, modified by diffusion (Hollister, 1969; Thompson, 1976; Spear, 1988).

Biotite around garnet and staurolite defining the main cleavage, has an usual X_{Fe} ratio (around 0.55–0.56) and a Ti content around 0.15–0.19 atoms per formula unit. White micas are essentially muscovite, comparable to the one analysed in the lower pelitic schists.

Chlorite is present in three different structural associations:

—as porphyroblasts associated with garnet;
—grown in the crenulation cleavage;
—as alteration products around garnet.

Analyses of the different chlorites show a very homogeneous composition with a Fe/(Fe + Mg) ratio close to 0.5 and a restricted range in Si variation (5.2–5.7 atoms per formula unit), corresponding to ripidolite.

Staurolite, with TiO_2 around 0.5 wt.% and a X_{Fe} ratio around 0.85–0.90, is similar to the staurolite in the lower contact. Plagioclase has limited compositional variation and consists of oligoclase-andesine (An_{25-40}). Apatite appears in pelitic schists, where iron oxide is also common; commonly cores of magnetite are rimmed by ilmenite.

3.4. Contact 7

The northernmost contact is exposed between the Glacier Blanc and the Glacier Noir. It appears as a very flat contact gently dipping towards the east and metamorphosing Liassic marbles with an apparent thickness of some 20–30 m. The foliation is defined by a very thin (millimeter scale) layering of quartz and calcite. Contact metamorphic minerals consist of porphyroclastic clinopyroxene + K-feldspar + plagioclase + scapolite ± chloritoid (Fig. 3e). Scapolite is surrounded by a coronitic intergrowth of clinozoisite + plagioclase + calcite suggesting the development of the reaction:

$$Scp + H_2O = Czo + Pl + Ca \quad (2)$$

Quartz grains show evidence of intracrystalline ductile deformation with reduction of grain size and extreme banded undulatory extinction. Such features suggest syntectonic recrystallization at low to moderate temperature (Gapais and Barbarin, 1986) associated with drag folds towards the northeast. The calc-silicate minerals have similar compositions to those described before.

4. Thermodynamic calculations

Calibrations of continuous and discontinuous reactions in the KMFASH system provide a good evaluation of the P–T conditions in pelitic schists (Thompson, 1976; Ferry and Spear, 1978; Hodges and Spear, 1982; Powell and Holland, 1985; Spear, 1988; Spear and Cheney, 1989). The occurrence of pelitic schists in the contact aureole at the base (contact 1) as well as at the roof of the granite (contact 6) provides a good opportunity to try to estimate temperature and pressure at the time of granite emplacement. We chose nine metapelitic samples (three at contact 1 and six at contact 6) where apparent textural equilibrium between thermobarometrically important minerals and lack of evidence for late-stage, low-T retrogression are observed. The absence of significant zoning in garnet support this assumption. The estimations of P–T conditions of granite emplacement is generally difficult because the constituent minerals may continue to react during slow cooling history of the magmatic body (Florence and Spear, 1989; Hodges, 1991). However, in the case of the Manaslu, $^{40}Ar/^{39}Ar$ datations indicate very rapid cooling of the granite over the 650–300°C temperature interval in Late Oligocene to Middle Miocene times (Copeland et al., 1990; Guillot et al., 1994b). In this case, we assumed that rim compositions are most likely to record equilibrium with contiguous grains and are the more representative for the "peak" metamorphism.

In order to assess the validity of our estimations, we use three complementary methods: plotting of the mineral assemblages in a partial petrogenetic grid of the KFMASH system (K_2O, FeO, MgO, Al_2O_3, SiO_2, H_2O); conventional thermobarometry computed by Spear et al. (1991) using rim mineral compositions—the theoretical background of this program is discussed in a short course note (Spear, 1989); and the *Thermocalc* computer program, based on an internally consistent thermodynamic dataset, presented by Powell and Holland (1985) and Holland and Powell (1990). This program has two major advantages over conventional themobarometry: it identifies all possible reactions between given endmember phases, calculating pressure or temperature with all relevant geothermometers or geobarometers, and it gives uncertainties based on the propagation of analytical uncertainties. The absence of

plagioclase and biotite inclusions in garnet prevents the application of inclusion thermobarometry.

Estimations of fluid conditions during metamorphism is a problem. Many reactions involving hydrous minerals are sensitive to water activity: the temperature may vary by up to 100°C between water-saturated and fluid-absent conditions. In the case of the Manaslu, we have made the following observations.

(1) All along the contact, the occurrence of a wide variety of parageneses with hydrated minerals (amphibole, clinozoisite, chlorite, micas, scapolite and tourmaline) indicates the presence of a H-O-C-B-F fluid phase.

(2) CO_2-rich fluids seem to be controlled by the local chemistry of rocks. In calcareous rocks at the contact, increase of temperature induces a series of decarbonatation reactions releasing H_2O as well as CO_2. The occurrence at contact 6 of calcic-rich scapolite suggests the importance of CO_2 in such rocks (Aitkens, 1983; Moecher and Essene, 1991), but its importance seems to be spatially limited.

(3) H_2O-rich fluids, on the contrary, seem to be widespread all along the rim of the granite where the metamorphic parageneses contain hydrated minerals. In pelitic schists, chlorite is stable, suggesting an elevated X_{H_2O}, superior to 0.8 according to thermodynamic calculation (see Grambling, 1990) and a relatively high f_{O_2} marked by the occurrence of hematite-quartz

Table 2
Thermobarometry for samples discussed in text, using the *Thermocalc* computer of Powell and Holland (1985) and Holland and Powell (1990)

Temperature (°C)

Sample	Assemblage	Contact	*Thermocalc*	Grt-Bt	Grt-St	Grt-Chl
D60	Grt + Bt + Ms + St + Pl	1	590 ± 50	550 ± 20	580 ± 30	
D73	Grt + Bt + Ms + Sil + Pl	1	540 ± 40	540 ± 20		
D74	Grt + Bt + Ms + Pl	1	580 ± 40	660 ± 90		
U472	Grt + Bt + Ms + Chl + Pl	6	560 ± 30	550 ± 30		520 ± 30
U453	Grt + Bt + Ms + Pl ± Chl	6	510 ± 40	560 ± 20		510 ± 30
U468	Grt + Bt + Ms + St + Pl	6	570 ± 60	530 ± 20	560 ± 20	
U480	Grt + Bt + Ms + St + Pl ± Chl	6	570 ± 50	540 ± 30	560 ± 20	490 ± 50
XG3	Grt + Bt + Ms + Pl	6		550 ± 20		
XG4	Grt + Bt + Ms + Pl	6		540 ± 20		

Pressure (MPa) Grt-Pl-Bt

Sample	Assemblage	Contact	*Thermocalc*	Ms ± Sil
D60	Grt + Bt + Ms + St + Pl	1	540 ± 110	500 ± 50
D73	Grt + Bt + Ms + Sil + Pl	1	500 ± 120	500 ± 50
D74	Grt + Bt + Ms + Pl	1	580 ± 80	590 ± 110
U472	Grt + Bt + Ms + Chl + Pl	6	340 ± 60	400 ± 30
U453	Grt + Bt + Ms + Pl ± Chl	6	280 ± 80	350 ± 30
U468	Grt + Bt + Ms + St + Pl	6	330 ± 100	350 ± 30
U480	Grt + Bt + Ms + St + Pl ± Chl	6	330 ± 100	300 ± 80
XG3	Grt + Bt + Ms + Pl	6		310 ± 30
XG4	Grt + Bt + Ms + Pl	6		320 ± 30

The thermometer garnet-biotite is from Ferry and Spear (1978), Hodges and Spear (1982) modified by Spear et al. (1991) to include the Hodges and Crowley (1985) garnet activity model. The garnet-biotite calibrations of Ganguly and Saxena (1984) and Perchuk and Lavent'eva (1984) are also used. The garnet-staurolite thermometer is from Perchuk (1969) whereas three calibrations of the garnet-chlorite thermometer are used (Dickinson and Hewitt, 1986; Ghent et al., 1987; Grambling, 1990). The garnet-biotite-muscovite-plagioclase barometer is from Ghent and Stout (1981) and Hodges and Crowley (1985) and the garnet-biotite-muscovite-plagioclase-sillimanite barometer is from Newton and Haselton (1981), Ganguly and Saxena (1984) and Hodges and Crowley (1985).

veins in the foliation plane. The occurrence of wollastonite indicates the infiltration of a H_2O-rich fluid as, at the temperature of contact metamorphism (550 ± 40°C, see the estimations below), wollastonite is not stable below $X_{H_2O} \approx 0.95$ (Flowers and Helgeson, 1983). The occurrence of clinozoisite in calcareous metasandstones suggests a H_2O-rich fluid (Nitsch and Store, 1972; Ferry, 1976; Chatterjee, 1976). Similarly, in calc-silicate rocks at the highest contact, scapolite is surrounded by a coronitic texture with clinozoisite-plagioclase-calcite implying the percolation of H_2O-rich fluid.

(4) The accumulation of tourmaline in the vicinity of the contact and its widespread occurrence in the aureole, reflects the flux of a volatile-rich H_2O fluid from the granite (Pichavant and Manning, 1984), and its diffusion throughout the aureole by infiltration during crystallization of the magma (Cartwright and Valley, 1991).

For these reasons, we have assumed conditions of a_{H_2O} close to 1 in pelitic schists.

P–T estimates for contact aureole pelitic schists samples are summarized in Table 2.

4.1. Thermobarometry at contact 6

Temperature has been estimated with the garnet + chlorite thermometer, based upon Fe–Mg exchange between the two minerals (Dickinson and Hewitt, 1986; Ghent et al., 1987; Grambling, 1990) and the garnet-biotite thermometer (Ferry and Spear, 1978; Hodges and Spear, 1982; Ganguly and Saxena, 1984; Perchuk and Lavent'eva, 1984).

In the garnet + chlorite + biotite assemblage (U472), where chlorite porphyroblasts are in textural equilibrium with garnet, the calculated temperatures range from 490 to 540°C. The garnet + biotite thermometer gives a higher value at 560 ± 30°C in the same sample.

The garnet + biotite assemblage (without staurolite or chlorite, sample U453, XG3 and XG4) yields temperatures ranging from 540 to 580°C, using the garnet + biotite themometer, and 510 ± 40°C with *Thermocalc* program.

In the staurolite + garnet ± chlorite assemblage (U468 and U480), the garnet + chlorite thermometer yields a large range of temperature between 440 and 540°C suggesting that chlorite is

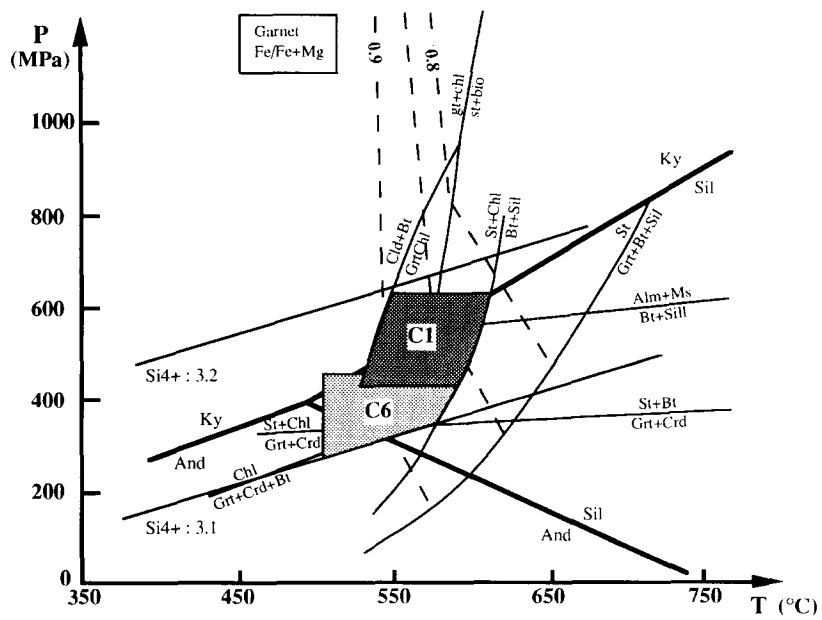

Fig. 6. Partial petrogenetic grid in the KFMASH system after Thompson (1976), Vielzeuf (1984) and Spear and Cheney (1989). The Fe/(Fe + Mg) ratio comes from Spear and Cheney (1989). *C1* = *P–T* area for contact 1; *C6* = *P–T* area for contact 6.

unstable when staurolite is present. In fact, with increase of temperature, garnet and chlorite become unstable together and, in the presence of muscovite give staurolite, according to reaction (Fig. 6):

$$Grt + Chl + Ms = St + Bt + Qtz + H_2O \quad (3)$$

This evolution is supported by the trend of zoning in garnet associated with staurolite and chlorite in the sample U468 (Fig. 4d); increase of almandine component and decrease of spessartine from core to rim result from the consumption of garnet during reaction (3) (Spear, 1988, 1989; Spear et al., 1990). According to the calibrations of Richardson (1968), Hoschek (1969), Ganguly (1972), Thompson (1976), Rao and Johannes (1979) and Dutrow and Holdaway (1989), the occurrence of staurolite in pelitic schist suggests a temperature minimum of 550–570°C and a maximum of 700°C at 300 MPa. The different thermometers yield values close to the minimum: 540 ± 30°C for garnet + biotite, 560 ± 20°C for the calibration of Perchuk (1969) on Fe–Mg exchange between garnet and staurolite, and 570 ± 50°C for *Thermocalc*.

The equilibrium assemblage garnet + plagioclase + biotite + muscovite allows us to estimate pressure conditions using the calibrations of Ghent and Stout (1981) and Hodges and Crowley (1985). These calibrated barometers are based on the exchange of CaO, K_2O, FeO, MgO, Al(VI) in the four minerals. At contact 6, they yield a pressure between 250 and 400 MPa with an average of 310 ± 80 MPa. In addition, the absence of Fe-cordierite in the staurolite-bearing gneisses indicates that pressure remained high during granite emplacement; a minimal pressure of 320 MPa can be estimated from the discontinuous reaction of Thompson (1976) (Fig. 6):

$$St + Bt = Grt + Crd \quad (4)$$

The *Thermocalc* pressure estimations (Table 2) give 340 ± 60 MPa for garnet + chlorite + biotite assemblages (U472), 280 ± 80 MPa for garnet + biotite assemblages (U453) and 330 ± 100 MPa for garnet + staurolite ± chlorite assemblages (U468 and U480).

4.2. *P–T estimations at contact 1*

Parageneses of the lower Palaeozoic schists represented in the KFMASH petrogenetic grid (Fig. 6) allow to estimate the pressure–temperature interval. The garnet + staurolite + biotite + muscovite ± chlorite assemblage (D60) without sillimanite is limited by reactions (3) and (5):

$$Grt + Chl + Ms = St + Bt + Qtz + H_2O \quad (3)$$

$$St + Chl + Ms = Bt + Sil + Qtz + H_2O \quad (5)$$

They bracket the temperature between 550 and 650°C and the pressure between 300 and 600 MPa in the sillimanite field.

Using the garnet-biotite geothermometers the staurolite-bearing schist D60 gives 550 ± 20°C whereas the sillimanite-bearing schist D73 without staurolite gives a temperature estimation of 540 ± 20°C. Sample D74 gives higher value around 660 ± 90°C, but the unusual composition of this pelitic schist interlayed in calc-silicate gneisses suggest that this result is doubtful. *Thermocalc* somewhat scatters the values obtained by petrogenetic grid and geothermometry: D73 gives 540 ± 40°C, D60 gives 590 ± 50°C and D74 gives an estimation of 580 ± 40°C.

The garnet + sillimanite + biotite + muscovite + quartz assemblage is limited by the reaction:

$$Grt + Ms = Sil + Bt + Qtz \quad (6)$$

suggesting a pressure lower than 600 MPa (Vielzeuf, 1984), whereas the garnet + staurolite + biotite + muscovite assemblage (D60), in absence of cordierite, suggests a pressure greater than 320 MPa (reaction 4). Moreover, considering the Si^{4+} content of white micas (Velde, 1967; Massone and Schreyer, 1986), the pressure estimations can be narrowed in the samples between 450 and 550 MPa in the 550–600°C temperature range.

The *Thermocalc* program gives a pressure range between 500 ± 124 and 580 ± 80 MPa on the different samples whereas the garnet + plagioclase + biotite + muscovite barometers on D60 and D74 give, respectively, 500 ± 50 and 590 ± 110 MPa. As for the temperature estimations, the highest pressure obtained for D74 is probably due to the high CaO content in plagio-

clase, outside the calibration range of garnet-plagioclase barometers. For the sillimanite-bearing schist D73, the garnet + plagioclase + sillimanite barometers of Newton and Haselton (1981), Ganguly and Saxena (1984) and Hodges and Crowley (1985) give a pressure estimation at 500 ± 50 MPa. According to these estimations, the average pressure at the base of the pluton is evaluated at 540 ± 100 MPa.

4.3. *P–T in calc-silicate gneisses and calcareous metasandstones*

In calc-silicate rocks and metasandstones, pressure is rather difficult to estimate, due to the absence of accurate *P–T* calibrating reactions and to the large influence of P_{H_2O}/P_{CO_2}.

In calc-silicate gneisses, the critical mineral assemblage being absent, only the occurrence of scapolite and accessory wollastonite close to the contact enables us to evaluate the minimal temperature conditions with large uncertainties. At high temperature in calcite-bearing rocks, scapolite is more stable than plagioclase according to reaction:

$$3An + Cal = Me \quad (7)$$

whereas, in the presence of quartz and calcite, clusters of wollastonite imply the reaction:

$$Cal + Qtz = Wo + CO_2 \quad (8)$$

Wollastonite is not a good thermometer due to its dependence on P_{CO_2}, nevertheless, crystallization of wollastonite in the first meters (< 10 m) surrounding the granite suggests temperatures around 600 ± 50°C probably during H_2O infiltration (Greenwood, 1967; Flowers and Helgeson, 1983).

The occurrence of scapolite from contact 2 to the upper Liassic contact 7, suggests a minimum temperature of 550°C (Ellis, 1978; Aitkens, 1983; Oterdoom and Gunter, 1983; Moecher and Essene, 1991). The ratio Ca/Na in the solid-solutions marialite (Na endmember) and meionite (Ca endmember) is temperature dependent. Except for one sample XG114 on contact 5, scapolite displays an almost constant composition all along the contact (X_{Me} from 0.75 to 0.77), and coexists with oligoclase-andesine plagioclase (An_{33}–An_{44}). From Aitken (1983), the mizzonite scapolite (Me_{75}) has the largest *T* and CO_2 stability field, due to an increase of Al–Si order (Moecher and Essene, 1990) and coexists with a wide variety of plagioclase composition (An_{30}–An_{100}). However, the study of Ferry (1976) in metamorphic calcareous sediments shows that for a composition range similar to ours (An_{34} and Eqan around 0.65), the temperature is around 560–600°C. This range of temperature is consistent with the previous estimations for the pelitic schists at contacts 1 and 6.

Finally, the occurrence of clinopyroxene-K-feldspar-plagioclase-calcite-quartz ± muscovite suggests the breakdown of the muscovite-calcite-quartz assemblage (observed far from the granite) according to the reaction:

$$Ms + Cal + 2Qtz = Or + An + CO_2 + H_2O \quad (9)$$

and the breakdown of calcic-amphibole according to:

$$Hbl + Cal + Qtz = Di + H_2O + CO_2 \quad (10)$$

Reaction (9) yields a minimal temperature of 570°C (Hewitt, 1973), whereas the crystallization of diopside implies a temperature over 500–530°C (Ferry, 1976) at a moderate CO_2/H_2O ratio of around 0.4 to 0.6.

Particularly at contact 5, where calcareous metasandstones are abundant, the amphibole + clinozoisite + plagioclase + calcite + quartz assemblage suggests the reaction:

$$Pl + Chl + Cal + Qtz = Hbl + Czo + H_2O + CO_2 \quad (11)$$

In the *P–T* grid of Plyusnina (1982) based on experimental calibration of amphibole and plagioclase, the plot of two samples of contact 5 (XG110 and XG117) gives the same range of temperature ($580 < T < 600$°C) for a pressure around 500 MPa. Though the temperature estimations seem to be realistic, with the occurrence of scapolite in the same samples and diopside in the calc-silicate gneisses, the pressure is rather too high. In contrast, the diagram of Raase (1974) based on the concentration of Si and Al(VI) in

the same analysed amphiboles indicates pressure of less than 500 MPa.

5. Discussion

5.1. Thermal evolution

From contacts 4 to 7, on the flank and top of the granite, the metamorphic evolution reflects only the emplacement of the granite in a rather cold environment that has experienced anchizonal to light greenschist regional conditions, from top to bottom. In contacts 1 and 2 at the base, and to a lesser extent, in contact 3 on the lower part of the flank, the situation is more complex, as the rocks have experienced amphibolite regional metamorphism before the emplacement of the Manaslu pluton. In this latter case, field and microscopic structural analysis enable to distinguish the two metamorphisms.

From base to top, the thermometry suggests that temperature was controlled in the aureole by the thermal effect of the Manaslu granite emplacement. In the two or three first meters from the contact, temperature reached 580–600°C, except at the apex of the granite, where wollastonite garnet-staurolite or garnet-sillimanite pelitic schists are lacking. Away from the contact (10–20 m), the temperature decrease to around 550°C, marked by the occurrence of clinopyroxene-K-feldspar-scapolite in calc-silicates, amphibole-clinozoisite-plagioclase in calcareous metasandstones and garnet-biotite-plagioclase ± chlorite in pelitic schists. The contact aureole, very narrow ($\sim$ 30 m) at the roof of the granite, increases towards the base. There, the contact metamorphism merges with the regional HT metamorphism M_2 estimated at around 500–550°C (Schneider and Masch, 1993). Concurrently, the microstructural observations suggest a change in the temperature/deformation evolution from base to top during granite emplacement: at the base, characteristic minerals of high temperature (i.e., sillimanite, biotite, muscovite in pelitic schists; scapolite, pyroxene and K-feldspar in calc-silicate rocks) define the new foliation plane and N70–80° lineation (Guillot et al., 1993). The earlier schistosity S_1, probably related to the northward back-folding (Colchen et al., 1986; Guillot et al., 1993), is completely transposed, implying that temperature remained high during deformation ($>$ 500°C in the sillimanite field according to Holdaway, 1971). This evolution is obvious up to contact 6.

Higher up in the series, at contact 6, crystallization of metamorphic minerals (principally garnet and staurolite) occurs during the transposition of the earlier schistosity S_1 by the new foliation plane S_2 (Fig. 3d), corresponding to a local flattening at the roof of the granite (Guillot et al., 1993). At the apex of the pluton, at contact 7, the main cleavage even postdates the high-temperature contact mineral assemblage (Fig. 3e) suggesting that the deformation proceeded at lower temperature during the rapid cooling of the magmatic body by unroofing of the cover towards the northeast (Guillot et al., 1993).

The crenulation cleavage S_3 is only recorded in the upper pelitic schists. It corresponds to a local ballooning of the granite during its emplacement and refolds the flattening plane S_2, without change in the direction of regional deformation. In this place, the distribution of minerals suggests a horizontal gradient of temperature contemporaneous with the deformation (Guillot et al., 1991). In the staurolite-bearing rocks, staurolite continued to grow during the beginning of S_3 development, whereas in the chlorite- and/or garnet-bearing rocks, a new chlorite crystallized. This evolution implies that close to the granite, temperature remained high during the growth of the strain slip, whereas farther from the granite ($\approx$ 20–50 m), it allowed only for the crystallization of chlorite.

5.2. Barometric implications

Pressure estimations are always difficult to assess with the required precision. In our case we want to address two different problems: that of the pressure at the time of emplacement, and that of the difference in pressure between the bottom and the top of the pluton.

Pressure estimates at the upper and lower contacts overlap (Fig. 6), making it difficult to

establish pressure differences between the two. However, in order to minimize the error, we can compare the evaluations obtained on very similar rocks from the top and the bottom, with the same paragenesis, and using the same thermobarometer. This is the case for samples D60 (contact 1), and U468 and U480 (contact 6), with Grt + Bt + Ms + St + Pl + Qtz assemblages, using the Grt-Pl-Bt-Ms barometer of Ghent and Stout (1981) and Hodges and Crowley (1985) (see Table 2). The pressure difference varies from a minimum of 70 MPa to a maximum of 330 MPa. The estimation of 8 km of structural thickness between the base and top contacts (1 and 6) based on field observations (Le Fort, 1981), equivalent to a lithostatic pressure difference of 220 MPa, falls in the bracket. It provides an independent check on the thickness of the pluton and demonstrates that the pluton has not been thinned greatly since their emplacement. Unfortunately, the lack of pelitic schists at the lateral contacts prevents from refining statiscally the pressure evolution along the contact. Yet, the pressure recording cannot be strictly contemporaneous along the entire contact of a cooling pluton, 8 km thick, and hence, the estimation of pressure difference is blurred by another uncertainty.

As for the depth of granite emplacement, the pressure estimations at the top, using a density of 2.7 g/cm^3 for the overlying series, yield values of 9–13 km for the roof, and 18–21 km for the base. Such a depth of emplacement appears important, particularly for a leucogranite, commonly emplaced at shallow levels. For instance, the late Hercynian leucogranites of Western Europe were emplaced at depth shallower than 10 km (Giulani, 1982; Dahamani, 1985; Lagarde, 1989).

The roof of the Manaslu granite intrudes the Upper Triassic and Liassic; the overlying series, from Dogger to Upper Cretaceous, have an estimated stratigraphic thickness of 3000 m (Colchen et al., 1986). This stratigraphic thickness is three to four times less than that implied by the barometric calculations. This difference may be explained in two ways: a large refolding of the Higher Himalayan Sedimentary Series (HHSS) and/or a nappe emplacement by a thrust fault.

The first interpretation would be supported by the development of large northward-verging folds in the Manaslu area. Structural studies have demonstated that the granite emplacement postdates these folds (Guillot et al., 1993). However, in the Annapurna range, 50 km east of the Manaslu massif, Boullier et al. (1991) have shown an increase in pressure of 40 to 100 MPa recorded by fluid inclusions in stratigraphic levels equivalent to those of the present area. They explain this increase by the burial of the HHSS by the

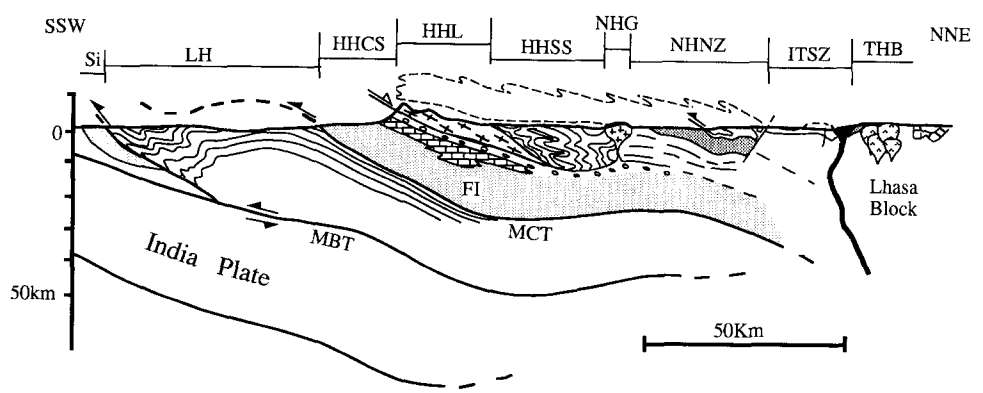

Fig. 7. Schematic cross section of (a) the present structure of the Himalaya in Central Nepal and (b) the minimal extension of nappes during the Miocene (dashed line). Modified after France-Lanord and Le Fort (1988). *HHCS* = Higher Himalayan Crystalline Series (Tibetan Slab); *HHL* = High Himalayan leucogranite (Manaslu); *HHSS* = Higher Himalayan Sedimentary Series; *ITSZ* = Indus–Tsangpo Suture Zone; *LH* = Lesser Himalaya; *MBT* = Main Boundary Thrust; *MCT* = Main Central Thrust; *NHG* = North Himalaya Granite; *NHNZ* = North Himlaya Nappe Zone; *Si* = Siwaliks; *THB* = Transhimalaya Batholith; *FI* = Formation I of the *HHCS*.

development of the northward-verging folds. Nevertheless, the refolding of the cover is insufficient to explain the 330–530 MPa records in the contact aureole of the Manaslu granite.

The second interpretation is based on the development of large nappes in the North Himalayan domain: southern Tibet (Burg, 1983) and Zanskar (Honegger, 1983). Northeast of the Manaslu, Burg (1983), Burg et al. (1984) and Brunel and Kienast (1986) mapped and discussed a major thrust fault, the Kangmar thrust, that would have also thickened the crust prior to the MCT thrusting. Far to the west, in Garwhal, Hodges and Silverberg (1988) have suggested that the entire Greater Himalaya underwent a miminimum burial of 5 km during the high-temperature metamorphism M_2 event in the Late Oligocene. They proposed to relate the M_2 event to the leucogranite injection, the burial being related to thrusting on a presently unexposed fault, north of the High Himalayan leucogranites.

Thus, we suggest that the 50 km wide North Himalayan nappes, known in the southern part of the Indus–Tsangpo suture, would have extended towards the south for an additional minimum of 70 km during Miocene times (Fig. 7). To explain the burial recorded in the contact aureole of the Manaslu granite, their thickness must have been at least 7–10 km. These are probably miniminum values, as their emplacement began at 55–50 Ma (Le Fort, 1989), and they were probably in part eroded 30 Ma later, at the time of granite emplacement. During the first 30 Ma, the nappe emplacement was probably responsible for the Eo-Himalayan metamorphism recorded in the Higher Himalayan Crystallines (Caby et al., 1983; Le Fort, 1989; Pêcher, 1989; England et al., 1992).

This tectono-metamorphic study shows that the normal fault zone at the base of the HHL and the northward-verging Annapurna fold predate for a large part the emplacement of the Manaslu body. This is supported by the occurrence of contact metamorphic minerals postdating the cleavage associated with the northward-trending folds. A similar situation has been reported in Langtang valley, northern Nepal, by Inger and Harris (1992) although this second heating event is explained by heat focusing at the top of the HHC.

The deep level of emplacement and young ages of the granite crystallization, around 25 Ma (Guillot, 1993), imply rapid denudation rates, in the order of 1 mm a^{-1} (see also Le Fort, 1988). As suggested by Caby et al. (1983), it requires tectonic denudation by normal faulting. Numerous authors have described large normal faulting north of the HHL (e.g., Burg, 1983; Burg et al., 1984; Gapais et al., 1984; Herren, 1987; Hodges et al., 1992), definitely postdating the HHL in a number of occurrences (e.g., Herren, 1987). The tectonometamorphic evolution of the Manaslu also supports this general scheme.

6. Summary and conclusion

Microstructural study and thermobarometrical investigation in the contact aureole of the Manaslu granite show that the massif was emplaced at a depth of 9–13 km for the roof and 18–21 km for the base with a temperature rather constant all along the contact at around 550 ± 40°C. The temperature remained high at the base of the massif, whereas cooling was more rapid at the top and unroofing occurred at lower temperature at the end of the granite emplacement obliterating in part the earlier ductile structures in the aureole. The great depth of emplacement implies large refolding of the cover and more probably the piling up of nappes before granite emplacement, followed by a rapid tectonic denudation by northward-trending normal faulting.

Acknowledgments

Field and laboratory work were supported by Commissariat à l'énergie atomique (C.E.A. contract MC:15.154) and Laboratoire de géodynamique des chaînes alpines (C.N.R.S., U.R.A. 69). The authors thank J.M. Lardeaux and E. Ghent for comments on an earlier draft. Fruitful suggestions and comments from R. Vernon and S. Elvevold have been greatly appreciated. We want to thank particularly F.S. Spear for its very constructive and helpful review.

References

Aitkens, B.G., 1983. $T-X_{CO_2}$ stability relations and phase equilibria of a calcic carbonate scapolite. Geochim. Cosmochim. Acta, 47: 351–362.

Boullier, A.M., France-Lanord, C., Dubessy Adamy, J. and Champenois, M., 1991. Linked fluid and tectonic evolution in the High Himalaya mountains (Nepal). Contrib. Mineral. Petrol., 107: 358–372.

Brunel, M. and Kienast, J.R., 1986. Etude pétro-structurale des chevauchements ductiles himalayens sur la transversale de l'Everest–Makalu (Népal oriental). Can. J. Earth Sci., 23: 1117–1137.

Burg, J.P., 1983. Tectogénèse comparée de deux segments de chaîne de collision: le sud du Tibet (suture du Tsangpo), la chaîne hercynienne en Europe (suture du Massif-Central). Thesis, Montpellier, 450 pp.

Burg, J.P., Brunel, M., Gapais, D., Chen, G.M. and Liu, G.H., 1984. Deformation of the leucogranites of the crystalline main central sheet in southern Tibet (China). J. Struct. Geol., 6: 532–542.

Caby, R., Pêcher, A. and Le Fort, P., 1983. Le grand chevauchement central himalayen: nouvelles données sur le métamorphisme inverse à la base de la Dalle du Tibet. Rev. Géol. Dyn. Géogr. Phys., 24: 89–100.

Cartwright, I. and Walley, J.W., 1991. Steep oxygen-isotope gradients at marble metagranite contacts in the northwest Adirondack Mountain, New-York, USA: products of fluid-hosted diffusion. Earth. Planet. Sci. Lett., 107: 148–163.

Chatterjee, N.D., 1976. Margarite stability and compatibility relations in the system $CaO-Al_2O_3-Si0_2-H_2O$ as a pressure–temperature indicator. Am. Mineral., 61: 699–709.

Colchen, M., Le Fort, P. and Pêcher, A., 1986. Recherches géologiques dans l'Himalaya du Népal. Annapurna, Manaslu, Ganesh. C.N.R.S., Paris, 136 pp.

Copeland, P., Harrison, T.M. and Le Fort, P., 1990. Age and cooling of the Manaslu granite: implications for Himalyan tectonics. J. Volcanol. Geotherm. Res., 44: 33–50.

Dahamani, A., 1985. Le métamorphisme dans l'auréole du granite d'Oulmés (Maroc Central): étude pétrographique et relations avec les déformations hercyniennes. Thesis, Rabat, 228 pp.

Deniel, C., Vidal, Ph., Fernandez, A., Le Fort, P. and Peucat, J.-J., 1987. Isotopic study of the Manaslu granite (Himalaya, Nepal): Inferences on the age and source of Himalayan leucogranites. Contrib. Mineral. Petrol., 96: 78–82.

Dickinson III, M.P. and Hewitt, D.A., 1986. A garnet-chlorite geothermometer. Geol. Soc. Am. Abstr., 18: 584.

Dutrow, B.L. and Holdaway, M.J., 1989. Experimental determination of the upper thermal stability of Fe-Staurolite + quartz at medium pressures. J. Petrol., 30: 229–248.

Ellis, D.E., 1978. Stability and phase equilibria of chloride and carbonate bearing scapolites at 750°C and 4000bars. Geochim. Cosmochim. Acta, 42: 1271–1281.

England, P., Le Fort, P., Molnar, P. and Pêcher, A., 1992. Heat sources for Tertiary metamorphism and anatexis in the Annapurna–Manaslu region (Central Nepal). J. Geophys. Res., 97: 2107–2128.

Ferry, J.M., 1976. P, T, f_{O_2} during metamorphism of calcareous sediments in the Waterville–Vassalvoro area, South-Central Maine. Contrib. Mineral. Petrol., 57: 119–143.

Ferry, J.M. and Spear, F.S., 1978. Experimental calibration of the partitioning of Fe and Mg between biotite and garnet. Contrib. Mineral. Petrol., 66: 113–117.

Florence, F.P. and Spear, F.S., 1989. Volume diffusion in garnet: effects on $P-T$ path calculations. EOS, 70: 492.

Flowers, G.C. and Helgeson, H.C., 1983. Equilibrium and mass transfer during progressive metamorphism of siliceous dolomites. Am. J. Sci., 283: 230–286.

France-Lanord, C. and Le Fort, P., 1988. Crustal melting and granite genesis during the Himalayan collision orogenesis. Trans. R. Geol. Soc. Edinburgh, 79: 183–195.

Frey, M., 1987. Low-Temperature Metamorphism. Elsevier, Amsterdam, 351 pp.

Ganguly, J., 1972. Staurolite stability and related parageneses: theory, experiments and applications. J. Petrol., 62: 335–365.

Ganguly, J. and Saxena, S.K., 1984. Mixing properties of aluminosilicates garnets: constraints from natural and experimental data, and applications to geothermobarometry. Am. Mineral., 69: 88–97.

Gapais, D. and Barbarin, B., 1986. Quartz fabric transition in a cooling syntectonic granite (Hermitage massif, France). Tectonophysics, 125: 357–370.

Gapais, D., Gilbert, E. and Pêcher, A., 1984. Structures et trajectoires de déformation dans la zone de suture de l'Indus–Tsangpo en Himalaya du Ladakh, région de la Suru. C. R. Acad. Sci. Paris, 299: 179–182.

Ghent, E.D. and Stout, M.Z., 1981. Geobarometry and geothermometry of plagioclase-biotite-garnet-muscovite assemblage. Contrib. Mineral. Petrol., 76: 86–97.

Ghent, E.D., Stout, M.Z., Black, M.P. and Brother, R.N., 1987. Chloritoïd-bearing rocks associated with blueschists and eclogites, northern New-Caledonia. J. Metamorph. Geol., 5: 239–254.

Giulani, G., 1982. Contribution à l'étude géochronologie du massif granitique des Zaer (Maroc Central). M.S. Thesis, Nancy, 250 pp.

Grambling, J.A., 1990. Internally consistent geothermometry and H_2O barometry in metamorphic rocks: the example garnet-chlorite-quartz. Contrib. Mineral. Petrol., 105: 617–628.

Greenwood, H.J., 1967. Wollastonite: stability in H_2O-CO_2 mixtures and occurence in a contact metamorphism aureole near Salmo, british Columbia, Canada. Am. Mineral., 52: 1669–1680.

Guillot, S., 1993. Le granite du Manaslu (Népal Central), marqueur de la subduction et de l'extension intracontinentale himalayenne (Thesis). Géol. Alpine 19, 97 pp.

Guillot, S., Le Fort, P. and Pêcher, A., 1991. Evolution métamorphique et microstructurale polyphasée de

l'auréole du granite du Manaslu (Népal Central). Bull. S.F.M.C., 2: 38 (abstract).

Guillot, S., Rochette, P., Le Fort, P. and Pêcher, A., 1993. The emplacement of the Manaslu granite (Central Nepal): field and magnetic susceptibility constraints. In: P.J. Treloar and M. Searle (Editors), Himalyan Tectonics. Geol. Soc. London Spec. Publ., 74: 413–428.

Guillot, S., Le Fort, P. and Pêcher, A., 1994a. Comparison of the emplacement of some High Himalayan Leucogranites. Mustang, Manslu and Kula–Kangri. J. Nepal Geol. Soc., 10: 101–102.

Guillot, S., Hodges, K.V., Le Fort, P. and Pêcher, A., 1994b. New constraints on the age of the Manaslu granite: evidence for episodic Oligo–Miocene tectonic denudation in Central Himalayas. Geology, 29: 559–562.

Harrison, T.M., Copeland, P., Kidd, W.S.F. and Yin, A., 1992. Raising Tibet. Science, 255: 1663–1670.

Herren, E., 1987. Zanskar shear zone: Northeast–southwest extension within the Higher Himalayas (Ladakh, India). Geology, 15: 409–413.

Hewitt, D.A., 1973. Stability of the assemblage muscovite-calcite-quartz. Am. Mineral., 58: 785–791.

Hodges, K.V., 1991. Pressure–temperature–time paths. Annu. Rev. Earth Planet. Sci., 19: 207–236.

Hodges, K.V. and Crowley, P.D., 1985. Error estimation and empirical geothermobarometry for pelitic systems. Am. Mineral., 73: 20–47.

Hodges, K.V. and Silverberg, D.S., 1988. Thermal evolution of the Greater Himalaya, Garhwal, India. Tectonics, 73: 583–600.

Hodges, K.V. and Spear, F.S., 1982. Geothermometry, geobarometry and the Al_2Si0_5 triple point at Mt. Moosilauke, New Hampshire. Am. Mineral., 67: 1118–1134.

Hodges, K.V., Burchiel, B.C., Chen, T., Lux, D. and Royden, L.H., 1992. Rapid early Miocene tectonic unroofing of the metamorphic core of the Himalaya: Simultaneous extension and shortening in the Himalayan Orogen. Science, 258: 1466–1470.

Holdaway, M.J., 1971. Stability of andalusite and the aluminium silicate phase diagram. Am. J. Sci., 271: 97–131.

Holland, T.J.B. and Powell, R., 1990. An enlarged and updated internally consistent thermodynamic dataset with uncertainties and correlations: the system K_2O–Na_2O–CaO–MgO–MnO–FeO–Fe_2O_3–Al_2O_3–TiO_2–SiO_2–C–H_2–O_2. J. Metamorph. Geol., 8: 89–24.

Hollister, L.S., 1969. Contact metamorphism in the Kwoiek area of British Columbia: an end member of the metamorphic process. Geol. Soc. Am. Bull., 80: 2465–2494.

Honegger, K., 1983. Strukturen und Metamorphose im Zanskar Kristallin (Ladakh–Kashmir, NW Himalaya). Ph.D. Thesis, ETH–Zürich, 351 pp.

Hoschek, G., 1969. The stability of staurolite and chloritoid and their significance in metmorphism of pelitic rocks. Contrib. Mineral. Petrol., 22: 208–232.

Inger, S. and Harris, B.W., 1992. Tectonothermal evolution of the High Himlayan Crystalline sequence, Langtang valley, northern Nepal. J. Metamorph. Geol., 10: 439–452.

Kretz, R., 1983. Symbols for rock-forming minerals. Am. Mineral., 68: 277–279.

Kwak, T.A.P., 1968. Ti in biotite and muscovite as an indicator of metamorphic grade in almandine amphibolite facies rocks from Sudbury, Ontario. Geochim. Cosmochim. Acta, 32: 1222–1229.

Lagarde, J.L., 1989. Granites tardi-carbonifère et déformation crustale. L'exemple de la Meseta Marocaine. Mém. Doc. CAESS, 350 pp.

Leake, B.E., 1978. Nomenclature of amphiboles. Can. Mineral., 16: 501–520.

Le Fort, P., 1981. Manaslu leucogranite: a collision signature of the Himalaya. A model for its genesis and emplacement. J. Geophys. Res., 86: 10,545–10,568.

Le Fort, P., 1988. Granites in the tectonic evolution of the Himalaya, Karakorum and southern Tibet. Philos. Trans. R. Soc. London, 326: 281–299.

Le Fort, P., 1989. The Himalayan orogenic segment. In: A.M.C. Sengör (Editor), Tectonic Evolution of the Tethyan Region. Kluwer Academic Publishers, Dordrecht, pp. 289–386.

Le Fort, P., 1991. Enclaves of the Miocene leucogranites. In: J. Didier and B. Barbarin (Editors), Enclaves and Granite Petrology. Elsevier, Amsterdam, pp. 35–46.

Le Fort, P., Cuney, C., Deniel, C., France-Lanord, C., Sheppard, S.M.F., Upretti, B.N. and Vidal, Ph., 1987. Crustal generation of the Himalayan leucogranites. Tectonophysics, 134: 39–57.

Massone, H.J. and Schreyer, W., 1987. Phengite barometry based on the limiting assemblage with K-feldspar, phlogopite and quartz. Contrib. Mineral. Petrol., 96: 212–224.

Moecher, D.P. and Essene, E.J., 1990. Phase equilibria for calcic scapolite and implications of variable Al–Si disorder for $P-T$, $T-X_{CO_2}$ and $a-X$ relations. J. Petrol., 31: 997–1024.

Moecher, D.P. and Essene, E.J., 1991. calculation of CO_2 activities using scapolite equilibria and composition of fluid phase during high grade metamorphism. Contrib. Mineral. Petrol., 108: 219–240.

Newton, R.C. and Haselton, H.T., 1981. Thermodynamics of the garnet-plagioclase-$Al_2Si_2O_5$-quartz geobarometer. In: R.C. Newton, A. Navrotsky and B.J. Wood (Editors), Thermodynamics of Minerals and Melts. Springer-Verlag, New York, NY, pp. 131–147.

Nitsch, K.H. and Storre, B., 1972. Zur Stabilität von Margarit in H_2O–CO_2 Gasgemischen. Fortschr. Mineral., 50: 71–73.

Oterdoom, H. and Gunter, W.D., 1983. Activity models for plagioclase and CO_3-scapolites: an analysis of field and laboratory data. Am. J. Sci., 283A: 255–282.

Patriat, P. and Achache, J., 1984. India–Eurasia collision chronology has implications for crustal shortening and driving mechanisms of plates. Nature, 311: 615–621.

Pêcher, A., 1989. The metamorphism in Central Himalaya. J. Metamorph. Geol., 7: 31–41.

Perchuk, L.L., 1969. The staurolite garnet thermometer. Dokl. Acad. Sci. USSR. Earth. Sci. Sect., 188: 189–191.

Perchuk, L.L. and Lavent'eva, I.V., 1984. Experimental inves-

tigation of exchange equilibria in the system cordierite-garnet-biotite. In: S.K. Saxena (Editor), Kinetics and Equilibrium in Mineral Reactions. Springer-Verlag, New York, NY, pp. 199–240.

Pichavant, M. and Manning, D., 1984. Petrogenesis of tourmaline granites and topaz granites; the contribution of experimental data. Phys. Earth. Planet. Inter., 35: 31–50.

Plyusnina, L.P., 1982. Geothermometry and geobarometry of plagioclase–hornblende bearing assemblages. Contrib. Mineral. Petrol., 80: 140–146.

Powell, R. and Holland, T.J.B., 1985. An internally consistent thermodynamic dataset with uncertainties and correlations: 1. Methods and worked example. J. Metamorph. Geol., 3: 327–342.

Raase, P., 1974. Al and Ti contents of hornblende indicators of pressure and temperature of regional metamorphism. Contrib. Mineral. Petrol., 45: 231–236.

Rao, B.B. and Johannes, W., 1979. Further data on the stability of staurolite + quartz and related assemblages. Neues Jahrb. Mineral. Monatsh., 10: 437–447.

Richardson, S.W., 1968. Staurolite stability in a part of the system K_2O–MGO–AL_2O_3. J. Petrol., 11: 73–99.

Schneider, C. and Masch, L., 1993. The metamorphism of the Tibetan Series from the Manang area, Marsyandi Valley, Central Nepal. In: P.J. Treolar and M. Searle (Editors), Himalyan Tectonics. Geol. Soc. London Spec. Publ., 74: 357–374.

Schreurs, J., 1985. Prograde metamorphism of metapelites, garnet-biotite thermometry and prograde changes of biotite chemistry in high-grade rocks of west Uusimaa, southwest Finland. Lithos, 18: 69–80.

Shaw, D.M., 1960. The geochemistry of scapolites. Part 1: previous work and general mineralogy. J. Petrol., 1: 218–260.

Spear, F.S., 1988. Metamorphic fractional crystallization and internal metasomatism by diffusional homogenization of zoned garnets. Contrib. Mineral. Petrol., 98: 507–517.

Spear, F.S., 1989. Petrologic determination of metamorphic pressure–temperature–time paths. In: F.S. Spear and S.M. Peacock (Editors), Metamorphic Pressure–Temperature–Time Paths, (Short course in Geology, 7) Am. Geophys. Union, Boulder, CO, pp. 1–55.

Spear, F.S. and Cheney, J.T., 1989. A petrogenetic grid for pelitic schists in the system SiO_2–Al_2O_3–FeO–MgO–K_2O–H_2O. Contrib. Mineral. Petrol., 101: 149–164.

Spear, F.S., Kohn, M.J., Florence, F.P. and Menard, T., 1990. A model for garnet and plagioclase growth in pelitic schists: implications for thermobarometry and P–T path determinations. J. Metamorph. Geol., 8: 683–696.

Spear, F.S., Peacock, S.M., Kohn, M.J., Florence, F.P. and Menard, T., 1991. Computer programs for petrologic P–T–t path calculations. Am. Mineral., 76: 2009–2012.

Stephenson, N.C.N., 1977. Coexisting hornblendes and biotites from Precambrian gneisses of the south coast of western Australia. Lithos, 10: 9–27.

Stern, C.R., Kriegfield, R., Schelling, R., Virdi, N.S., Futa, K., Peterman, Z.E. and Amini, H., 1989. The Bhagirathi leucogranite of the High Himalayas (Garhwal, India); age, petrogenesis, and tectonic implications. Geol. Soc. Am. Spec. Pap., 232: 33–46.

Thompson, A.B., 1976. Mineral reactions in pelitic rocks. Am. J. Sci., 276: 401–414.

Velde, B., 1967. Si^{4+} content of natural phengites. Contrib. Mineral. Petrol., 14: 250–258.

Vidal, P., Cocherie, A. and Le Fort, P., 1982. Geochemical investigations of the origin of the Manaslu leucogranite (Himalaya, Nepal). Geochim. Cosmochim. Acta, 46: 2279–2292.

Vielzeuf, D., 1984. Relations de phase dans le facies granulites. Thesis, Clermont-Ferrand, 198 pp.